Modeling and Analysis of AC Resistance of a Permanent Magnet Machine for Online Estimation Purposes

Shamsuddeen Nalakath, Matthias Preindl, Berker Bilgin, Bing Cheng, and Ali Emadi
Department of Electrical and Computer Engineering
McMaster University, Hamilton, Ontario, Canada

***Abstract*—A simple and accurate AC resistance model is essential for online estimation of copper loss which can be utilized in several ways of controlling and monitoring. This paper presents application of Squared Field Derivative on three-phase IPM machine to model AC resistance of rectangular conductors. It focuses on Finite Element Analysis to validate analytical model. The deviations from analytical model due to saturation and field weakening at high speeds are studied in detail and the significance of these deviations on the context of operating regions is discussed. This paper also presents application of the same analytical approach to model AC resistance of overhang conductors.**

I. Introduction

An electric traction motor operating in the extended speed range is employed in the transmission of electric and hybrid vehicles. It is possible to design and operate the machines for higher rated speed with the support of efficient power electronic devices and fast processors. With this design, the machine gets smaller and lighter. But the frequency dependent losses magnify accordingly. There are several techniques to reduce these losses at the design level[1][2]. Furthermore, these losses depend on the operating point and can be minimized online if estimated with sufficient precision [3]-[5]. Most of the techniques uses DC resistance to model the copper loss. Since AC resistance is substantially higher than DC resistance at high speed, it cannot be approximated with the latter one. A simple and accurate AC resistance model is necessary for online estimation. This model can also be applied in online temperature estimation. There are several methods available in the literature to model AC resistance [6]-[9]. However, models which are suitable for online estimation in the entire operating regime (high current and deep field weakening) are not well discussed.

The modeling of skin effect, which contributes to AC resistance, is relatively straight forward and has been well established [10][11]. The modeling of the proximity effect is complex due to peculiar magnetic structure and winding distribution of electric machines. However, the traditional proximity loss models used for transformers and inductors have been used for electric machines with a compromise on accuracy [12][13]. Reddy [6] compared traditional 1D model with strand-level 2D analytical model, which accounts for fringing at the slot opening. Unlike 1D model, the losses on the conductor, in proximity of the slot opening is closely matching with FEA results. In [7], an extension of this work was presented, where the same model is applied to estimate the bundle level proximity loss. An analytical model based on subdomain field is presented in [8] to estimate eddy current losses induced by magnetic field from magnet and coil excitation. The distribution of flux density in the slot by armature and rotor magnet excitations are integrated in [9] to find the total proximity loss. The conformal mapping technique is used for rotor magnet field and the model presented in [6] is used for armature excitation field. It is shown that proximity loss by rotor magnet field for a semi-open slot is negligible as compared to that by armature coil excitation field. Most of the above approaches need some level of computation which may not be suitable for online estimation.

The analytical model for proximity losses presented in this paper is based on Sullivan's Squared Field Derivative (SFD) method [14]. This method uses space averaged squared derivative of flux density which can be found by solving simple magneto-static problem, either by numerical or analytical methods. Its interaction with winding strands is calculated analytically to find proximity loss. This method is more time efficient than computing proximity loss numerically, and can be extended to multiple phases and 2D or 3D magnetic fields. The application of this approach, to find the proximity loss of an electric machine, has been presented in [15].

In this study, analytical method to find the space average square derivative of flux density in a slot was used. This paper briefly describes the same approach and apply to a single layer rectangular conductor three-phase winding of an IPM working in extended speed range. The values from analytical model are compared with FEA results. The effects of saturation and deep field weakening on proximity losses are discussed. This paper also investigates those effects in the contexts of different operating regions. Finally, the analytical model for AC resistance of overhang conductors is established by using the same analytical approach.

The analytical model for AC resistance which are presented in this paper can be implemented directly into an embedded platform. The model estimates the copper loss at different currents and speeds. The estimation scheme is shown in Fig. 1. The AC resistance model takes operating frequency and coil temperature as inputs and gives AC resistance as output. The copper loss is found by multiplying the AC resistance with

RMS of phase current.

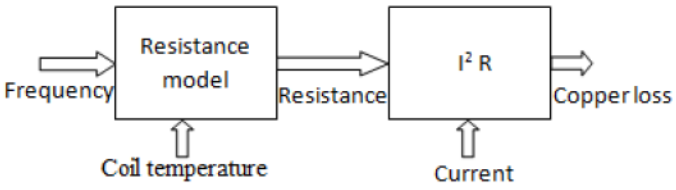

Fig. 1. Online estimation scheme.

In this paper the symbols <> and ¯ are stand for space and time averaged values respectively.

II. Analytical Model

The total eddy current loss in the conductors of an electrical machine from various sources is expressed as

$$P_{cu} = I^2(R_{dc} + R_{skin} + R_{proximity}) + P_{rotorflux} \quad (1)$$

$P_{rotorflux}$ is due to eddy current induced in the conductors by rotor magnetic field. This component is negligible for a well designed semi open slot machine [9][16] and it is not considered for analytical modeling in this paper. R_{skin} can be calculated using (2), which accounts for both DC and AC (by skin effect) resistances of a rectangular type of conductor per phase [15]. This equation is formed by first deriving the current density which expresses the voltage drop across the conductor (as $E = \frac{J}{\sigma}$), and the real component of impedance, which can found by dividing voltage drop by net current passing through the conductor. In (2), k_1 accounts for number of conductors and parallel paths in a phase, l is active length of a conductor, δ is skin depth, σ is conductance, and the other geometric details are shown in Fig. 2.

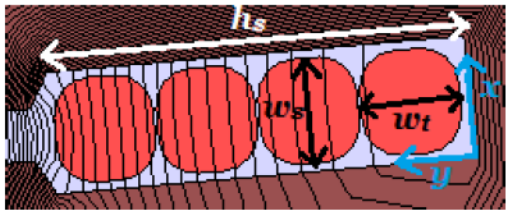

Fig. 2. Geometrical details and flux lines from FE of the slot.

$$R_{skin} = k_1 \frac{l}{\delta\sigma w_w(1-j)} \frac{e^{\frac{(1+j)w_t}{2\delta}} + e^{-\frac{(1+j)w_t}{2\delta}}}{e^{\frac{(1+j)w_t}{2\delta}} - e^{-\frac{(1+j)w_t}{2\delta}}} \quad (2)$$

The expression for proximity loss is developed by first deriving the copper loss ($i^2 r$) by eddy currents induced by magnetic field in x-direction (B_x) in elemental level of a conductor. Since the eddy current is proportional to derivative of B_x, $i^2\ r$ becomes proportional to squared derivative. By integrating throughout the conductor area [15], the conductor level loss can be calculated as in (3). It can be easily modified to get loss by y-direction field as well.

$$\overline{P} = \frac{1}{12}\ {w_t}^3\ w_w\ l\ \sigma\ \frac{1}{T}\int_0^T \left(\frac{dB_x}{dt}\right)^2 dt = C_x \overline{\left(\frac{dB_x}{dt}\right)^2} \quad (3)$$

Equation (3) can be modified to account all the conductors in a slot by by taking the space average of $(\frac{dB_x}{dt})^2$ throughout the area of a slot and multiplying by the number of conductors in a slot:

$$\overline{P_t} = N\ C_x\ \langle\ \left(\frac{dB_x}{dt}\right)^2 \rangle \quad (4)$$

In (4), the source of B_x is the armature-excited mmf and, hence, it is proportional to coil current. By normalizing with the current, B_x can be separated into $\hat{B}_x$ and $\frac{di}{dt}$. Therefore, (4) becomes

$$\overline{P_t} = N\ C_x\ \langle \hat{B}_x^2 \rangle (\frac{di}{dt})^2 \quad (5)$$

Equation (5) shows that, as $\langle \hat{B}_x^2 \rangle$ becomes independent of the excitation current and frequency. A simple magneto-static problem solved either by numerically or analytically is sufficient to find the solution.

If there are two mmf sources in a slot, say, phases u and w, which is the case in most electrical machines, the net averaged flux density can be found by adding flux density from two source ($\hat{B}_{xu}$ and $\hat{B}_{xw}$) as given below.

$$\begin{aligned} \langle \hat{B}_x^2 \rangle &= \langle \left(\hat{B}_{xu} + \hat{B}_{xw}\right)^2 \rangle \\ &= \langle \hat{B}_{xu}^2 + 2\ \hat{B}_{xu}\ \hat{B}_{xw} + \hat{B}_{xw}^2 \rangle \end{aligned} \quad (6)$$

By arranging the flux density components and current derivatives for phases u and w in a matrix form, the total proximity loss in a slot can be expressed as,

$$\begin{aligned} \overline{P_t} = C_x(N_u + N_w)\frac{d}{dt}\begin{bmatrix} i_u & i_w \end{bmatrix} \\ \langle \begin{bmatrix} \hat{B}_{xu}^2 & \hat{B}_{xu}\hat{B}_{xw} \\ \hat{B}_{xu}\hat{B}_{xw} & \hat{B}_{xu}^2 \end{bmatrix} \rangle \frac{d}{dt}\begin{bmatrix} i_u \\ i_w \end{bmatrix} \end{aligned} \quad (7)$$

The next step is to find the squared space average of flux density in the slot by individual phases and their combined fields. The expressions corresponding to different flux density components are given below.

$$\langle \hat{B}_{xu}^2 \rangle = \frac{1}{3}\left(\frac{\mu_0 N_u}{w_s}\right)^2 \quad (8)$$

$$\langle \hat{B}_{xw}^2 \rangle = \frac{1}{3}\left(\frac{\mu_0 N_w}{w_s}\right)^2 \quad (9)$$

$$\langle \hat{B}_{xu}\hat{B}_{xw} \rangle = \frac{1}{3}\left(\frac{\mu_0}{w_s}\right)^2 N_u\ N_w \quad (10)$$

The flux density in y-direction B_y is not considered in this paper as it is negligible, except the small flux fringing region near the slot opening as shown in Fig. 1.

By considering sinusoidal current excitation, and substituting (8)-(10) into (7), the total time averaged proximity loss is formed per phase as

$$\overline{P_t} = k_2\ \frac{{\mu_0}^2\ \sigma\ l\ {w_t}^3\ w_w\ I^2\ (N_u + N_w)}{36{w_s}^2}$$

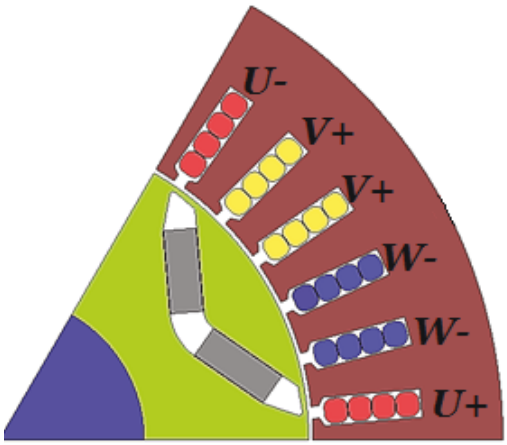

Fig. 3. IPM machine model considered in this paper.

TABLE I
MACHINE DETAILS

Rated output	10000 W
Rated speed	8000 rpm
DC link voltage	48V
Number of poles	6
Number of slots	36
Number of turns per phase	48

$$\left({N_u}^2 - N_u N_w + {N_w}^2\right) {w_e}^2 \tag{11}$$

where, w_e is excitation frequency, k_2 is the constant which accounts for number of conductors and parallel paths in a phase and I is the rms value of phase current. From (11), $R_{proximity}$ can be found by dividing it by I^2.

III. FINITE ELEMENT ANALYSIS

The 2D model of the reference IPM machine is shown in Fig. 3. The machine details are given in Table I. The machine has six poles and 36 slots. Each slot has four conductors of the same phase. A 2D Finite Element analysis is carried out in commercial software JMAG. The net phase resistance is estimated from the total joule losses in the conductors when they are excited by a three phase source without the rotor excitation applied in the FEA model. The estimated values at different excitation frequencies along with those from analytical model have very good correlations as shown in Fig. 4.

As the next step, the phase resistance is estimated from 2D FEA with both the rotor and the armature are excited together at different excitation angles (field weakening) and different armature currents. Only few steps are shown to make it convenient to explain. The excitation angle is varied from 0^o to 90^o with a step of 30^o and the current is varied from 50 A_{pk} to the maximum design value of the motor, 400 A_{pk}. The results are plotted in Fig. 5. The phase resistance from FEA is matching with analytical model at lower frequencies (50Hz and 300 Hz), and once the frequency increases to 600 Hz and 900 Hz, the values differ for lower excitation angles (0^o and 30^o). These deviations are due to interaction of rotor and

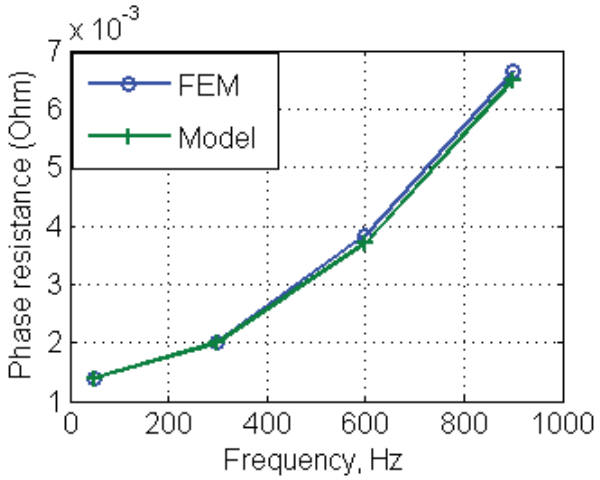

Fig. 4. Phase resistance vs excitation frequency.

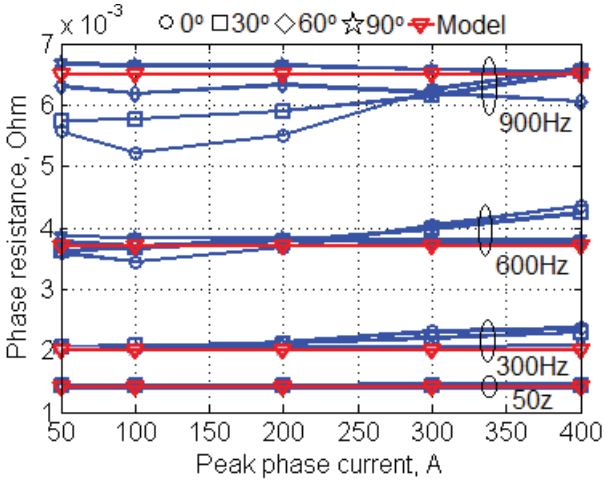

Fig. 5. Phase resistance for different excitation angles and currents.

armature field. The resultant flux leaves the rotor and enters the air gap with some angle from the radial axis. This results in concentration of flux in the top portion of the stator as shown in Fig. 6. The initial dip in the phase resistance in Fig. 5. at lower excitation angles is due to the saturation of the teeth by flux concentration. The following rise is attributed from the fact that the more flux crosses the conductors as the flux chooses nonmagnetic slot opening area as well at higher currents as shown in Fig. 7. This figure is taken at the first time step of transient simulation when U-phase conductors (in red color) are not excited, but still the flux crosses through them by other two phases. This results in additional eddy current loss.

At higher excitation angles (60^o and 90^o), the rotor and armature flux oppose each other, which results in pushing more armature flux (leakage) towards the slot as shown in Fig. 8. This leads to higher eddy current loss and results in higher phase resistance as plotted in Fig. 5.

The correlation between analytical model with FEA results at different frequencies, excitation angles and currents are

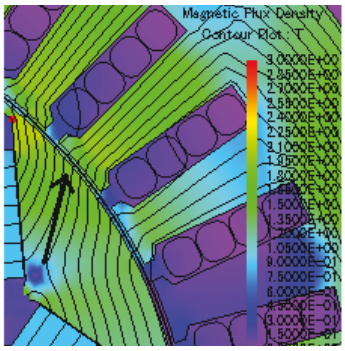

Fig. 6. Flux plot at 0^o excitation.

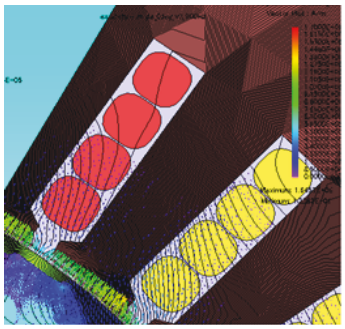

Fig. 7. Flux lines near slot opening at 0^o excitation and 200 A_{pk}.

Fig. 8. Flux lines at 90^0 excitation.

analyzed on the context of operating regions. In the starting region, where a machine operates at lower frequencies, lower angles and higher currents, the analytical model shows good correlation with FEA results between 50Hz and 300Hz as shown in Fig. 8. In the mid region, where the machine operates at nominal currents and lower field weakening, the model is highly correlated with the values corresponding to 50A, 100A, and 200A at 0^0 and 30^0, between 300 Hz and 700 Hz. Beyond 700 Hz, it shows deviation. However, the machine operates at deep field weakening region (60^o and 90^o) beyond 700 Hz, where the model shows good agreement with FEA results as shown in Fig. 10.

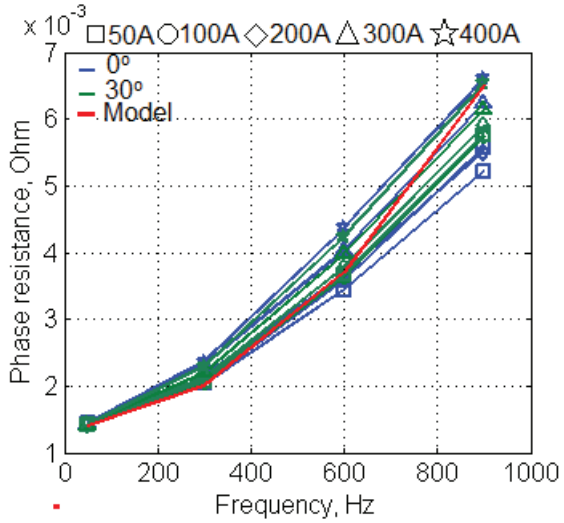

Fig. 9. Phase resistance at 0^0 and 30^0 excitations.

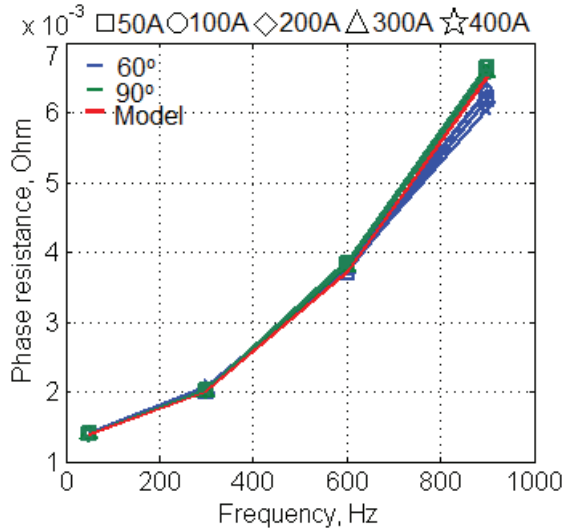

Fig. 10. Phase resistance at 60^0 and 90^0 excitations.

IV. Modeling AC Resistance of Overhang Conductors

The overhang conductors of a rectangular winding are generally arranged in a good pattern. Therefore, the electromagnetic field which is created by these conductors also shows some pattern. The understanding of this pattern can help to develop analytical model of resistance contributed by the proximity effect.

The overhang conductors of the reference machine are arranged in four layers. The coil switches its layer after half the coil pitch and then go to the next layer. First, the magnetic field distribution is studied by energizing only one coil. It is found that the conductors which are adjacent and parallel to the conductors of the energized coil in the same layer show more flux penetration and the conductors which cross over show less penetration as shown in Fig. 11 and Fig. 12 respectively.

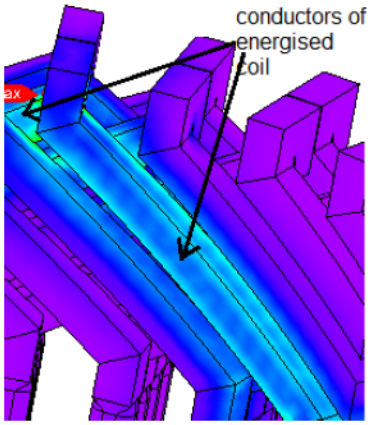

Fig. 11. The flux density plot showing the penetration in parallel conductors.

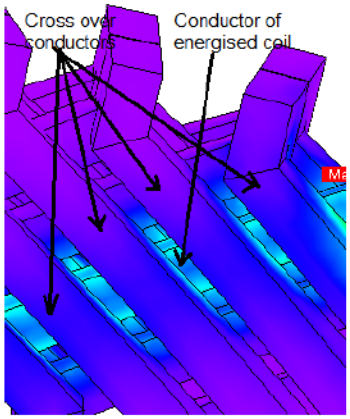

Fig. 12. The flux density plot showing the penetration in cross over conductors.

Figure 13 shows the time-averaged eddy current losses of all the coils in the overhang region when the coils of U-phase is only excited. Each bar in the graph corresponds to each coil. It is shown that only adjacent coils have considerable loss by the proximity effect.

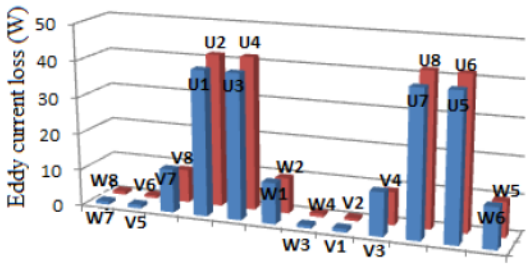

Fig. 13. The time averaged eddy current losses when only U phase is excited.

Based on the understanding of field distribution in the overhang region, it can be conceived that a conductor is electromagnetically influenced by the first adjacent conductors from each side in the same layer forming a group consists of three conductors. According to the winding pattern of the reference machine, two conductors of a group belong to one phase and the other two belong to another phase. In order to apply the same approach used in section II, the squared space average of flux density in the conductor has to be calculated. A circular flux pattern as shown in Fig. 14 is assumed in the region. The formulas for mid conductor by the field from two adjacent conductors belonging to two phases (u and v) are derived as

$$\langle \hat{B_{ru}}^2 \rangle = \frac{N_u (\frac{\mu_0}{2\pi})^2}{(D + \frac{w_w}{2})(D + \frac{3w_w}{2})} \tag{12}$$

$$\langle \hat{B_{rv}}^2 \rangle = \frac{N_v (\frac{\mu_0}{2\pi})^2}{(D + \frac{w_w}{2})(D + \frac{3w_w}{2})} \tag{13}$$

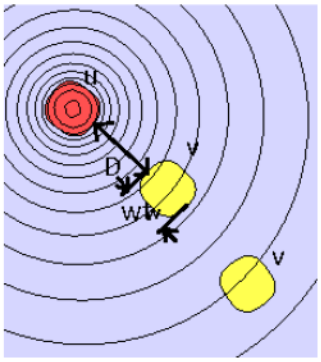

Fig. 14. Overhang conductor group.

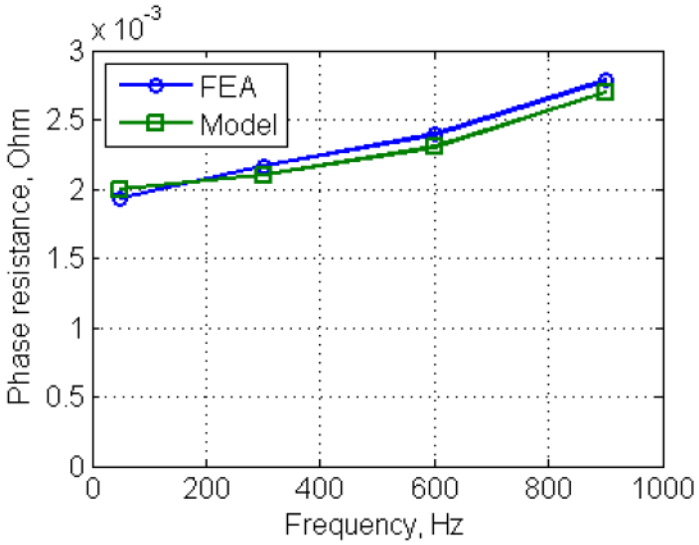

Fig. 15. Overhang conductor resistance per phase vs frequency.

As in section II, by substituting (12) and (13) in to (7) and considering the fact that $C_x = C_r$, the equation for proximity loss per phase becomes

$$\overline{P_{to}} = k_3 \frac{{\mu_0}^2 \ \sigma \ l_o \ {w_t}^3 \ w_w \ I^2 \ (N_u + N_v)}{48\pi^2 (D + \frac{w_w}{2})(D + \frac{3w_w}{2})}$$

$$(N_u{}^2 + N_u N_w + N_w{}^2)\ w_e{}^2 \quad (14)$$

where, N_u and N_v are u and v phase conductors in a group, '+' sign in $(N_u{}^2 + N_u N_w + N_w{}^2)$ is because of the field vectors of u and v phases are directly opposite in direction, k_3 is a constant which accounts for number of conductors and parallel path in a phase and l_o is half of coil length in one side of overhang region. Figure 15 shows that a good correlation exists between model and FEA values of the overhang phase resistance.

V. Discussions on Validation and Implementation

The AC resistance model presented in this paper is a function of frequency and machine details. It does not consider magnetic saturation and effect of different current excitation angles. The FE results at different current and angles for the reference machine are close to the model results. However, this can't be the case for other geometric types of machines. The model values may get deviated from the actual ones especially at higher currents and higher current excitation angles.

The AC resistance model presented in this paper is a simple and generalized one. It can be applied to any AC machines. However, the model has to be validated at different frequency, current and excitation angles. The accurate measurement of AC resistance at these conditions is a challenge as it is difficult to separate the iron and the AC copper losses from the total loss. The combination of FE and experimental results would be used to separate the losses [1] [17].

If the validation shows some discrepancy for the model, the correction factors can be introduced. The corrected model is then directly implemented into an embedded system. The estimated or measured coil temperature is required to update the resistance for temperature variation. The AC copper loss is estimated from AC resistance and RMS value of phase current.

VI. Conclusions

This paper identifies a simple analytical model for AC resistance estimation for real time control and monitoring purposes. It presents detailed FE analyses on validation of analytical model for the reference IPM machine. These analyses are resulted in describing the effects of saturation and field weakening on AC resistance. However, the uncertainties arised from these effects are acceptable for online estimation purposes. The approach used for modeling of proximity loss in active region is used to model for overhang region by understanding the distribution pattern of magnetic field. The analytical model shows good agreement with FEA results. The approach and analytical model presented in this paper can be applied to other machine geometries and topologies with validation by FEA, for the conditions mentioned in this paper.

VII. Acknowledgment

This research was undertaken in part, thanks from funding from the Canada Excellence Research Chair Program, Natural Sciences and Engineering Research Council of Canada (NSERC) and Automotive Partnership Canada (APC) Initiative. The authors also gratefully acknowledge Powersys solutions for their support with JMAG software in this research.

References

[1] P. H Mellor, R. Wrobel, N. McNeill,"Investigation of Proximity Losses in a High Speed Brushless Permanent Magnet Motor" , Industry Applications Conference, 2006. 41st IAS Annual Meeting, Vol. 2, pp. 1514-1518, October 2006.

[2] M. van der Geest, H Polinder, J. A. Ferreira, D. Zeilstra,"Stator winding proximity loss reduction techniques in high speed electrical machines", IEEE International Electric Machines Drives Conference (IEMDC), pp. 340-346, may 2013.

[3] A.S. Thomas, Z.Q. Zhu, G.W. Jewell,"Proximity Loss Study In High Speed Flux-Switching Permanent Magnet Machine," Magnetics, IEEE Transactions on , vol.45, no.10, pp.4748,4751, Oct. 2009.

[4] S. Vaez, V.I. John,M.A. Rahman, "An on-line loss minimization controller for interior permanent magnet motor drives," Energy Conversion, IEEE Transactions on , vol.14, no.4, pp.1435- 1440, Dec 1999.

[5] M.N. Uddin, F. Abera, "Online loss minimization based vector control of IPMSM drive," Electric Machines and Drives Conference, 2009. IEMDC '09. IEEE International , vol., no., pp.30,35, 3-6 May 2009.

[6] Z.Q.Zhu, Seok-Hee Han; , "Strand-level proximity losses in PM machines designed for high-speed operation," Electrical Machines, 2008. ICEM 2008. 18th International Conference on , vol., no., pp.1,6, 6-9 Sept. 2008.

[7] "Analysis of bundle losses in high speed machines," Power Electronics Conference (IPEC), 2010 International , vol., no., pp.2181,2188, 21-24 June 2010.

[8] L.J. Wu, Z.Q. Zhu, D. Staton, M. Popescu, ; D. Hawkins, "Analytical Model of Eddy Current Loss in Windings of Permanent-Magnet Machines Accounting for Load," Magnetics, IEEE Transactions on , vol.48, no.7, pp.2138,2151, July 2012.

[9] P.B. Reddy, T.M. Jahns, T.P. Bohn, "Modeling and analysis of proximity losses in high-speed surface permanent magnet machines with concentrated windings," Energy Conversion Congress and Exposition (ECCE), 2010 IEEE , vol., no., pp.996,1003, 12-16 Sept. 2010.

[10] Snelling, E.C., "Soft Ferrites - Properties and Applications", 1988(Second Edition).

[11] P.L. Dowell, "Effects of eddy currents in transformer windings", Proc. IEE, Aug 1966, vol. 113, No. 8, pgs. 1387-1394.

[12] R. E. Gilman, Eddy current losses in armature conductors, Trans. Amer. Inst. Elect. Eng., vol. XLIII, pp. 246251, Jan. 1924.

[13] A. B. Field, Eddy currents in large slot-wound conductors, Trans. Amer. Inst. Elect. Eng., vol. XXIV, pp. 761788, Jan. 1905.

[14] Sullivan, C.R., "Computationally efficient winding loss calculation with multiple windings, arbitrary waveforms, and two-dimensional or three-dimensional field geometry," Power Electronics, IEEE Transactions on , vol.16, no.1, pp.142,150, Jan 2001.

[15] S. Sudhoff, Power Magnetic Devices:A Multi-Objective Design Approach, Chapter 11, WILEY-IEEE PRESS,2014.

[16] Y. Deshpande, H. Toliyat, S. Nair, S. Dhinagar, S.Immadisetty, S. Nalakath, "High Torque Density Single Tooth-Wound Bar-Conductor Permanent Magnet Motor For Electric Two Wheeler Application," Industry Applications, IEEE Transactions on , vol.PP, no.99, pp.1,1.

[17] Wrobel, R.; Mlot, A.; Mellor, P.H., "Investigation of end-winding proximity losses in electromagnetic devices," Electrical Machines (ICEM), 2010 XIX International Conference on , vol., no., pp.1,6, 6-8 Sept. 2010.

[18] JSOL Corporation, JMAG, Chuo-Ku, Tokyo, Japan, 2013, [online], Available: http://www.jmag-international.com/.